ISSN 0021-3640, JETP Letters. ©Pleiades Publishing, Inc.,

Collisionless Plasma Processes at Magnetospheric Boundaries: Role of Strong Nonlinear Wave Interactions

S. Savin[a1)], E. Amata[b], L. Zelenyi[aj], C. Wang[c], H. Li[c], B. Tang[c], G. Pallocchia[b], J. Safrankova[d], Z. Nemecek[d], A. S. Sharma[e], F. Marcucci[b], L. Kozak[f], J. L. Rauch[g], V. Budaev[a,h], J. Blecki[i], L. Legen[a], M. Nozdrachev[a]

[a]Space Research Institute Russian Academy of Sciences, 117997 Moscow, Russia

[b]INAF-Istituto di Astrofisica e Planetologia Spaziali, 00133 Roma, Italy

[c]National Space Science Center, Chinese Academy of Sciences, 100190 Beijing, China

[d]Charles University, 1636 Prague, Czech Republic

[e]University of Maryland, College Park, 20742 Chesapeake, USA

[f]Kyiv Taras Shevchenko University, 01601 Kyiv, Ukraine

[g]Laboratory of Physics and Chemistry of the Environment and Space, 45071 Orleans, France

[h]NRC Kurchatov Institute, 123182 Moscow, Russia

[i]Space Research Center, 57622 Warsaw, Poland

[j]Moscow Physical Technical Institute, 12795 Moscow, Russia

Submitted 18 December 2018
Resubmitted 28 July 2019
Accepted 31 July 2019

This Letter presents an analysis of the sunward Poynting flux throughout magnetosheath and foreshock (directly measured by INTERBALL-1, CLUSTER-4 and DOUBLE STAR TC1) and its correlation and bi-correlation with the dynamic pressure of the solar plasma flow. It demonstrates, for the first time, that perturbations, caused by the resonances in the magnetospheric boundary layers, propagate upstream towards the bow shock as the short impulses of the sunward Poynting flux, which excite the strongest 3-wave resonances. They are initiated in the foreshock and regulate the bow shock surface oscillations. Another interaction zone near the magnetopause assists plasma flow extra deflection and acceleration around the magnetopause. At the outer boundary of stagnant cusp the turbulent barrier can separate the flowing and stagnant plasmas namely by the 3-wave cascades. So, both experiment and MHD modeling demonstrate the leading role of the discovered waves and nonlinear processes in the collisionless interaction of the plasma flow and magnetic barrier.

DOI: 10.1134/S0021364019170028

Background. Interaction of the variable solar wind (SW) plasma flow with the Earth's magnetosphere leads to the formation of the bow shock (BS), turbulent magnetosheath (MSH) downstream and magnetopause (MP = magnetospheric boundary). The resulting turbulence often becomes non-equilibrium one, non-steady and intermittent, accompanied by plasma jets with the dynamic pressure higher than that of the unshocked SW [1–3]. The low frequency eigen modes in the region bounded by the bow shock and magnetopause range from surface and cavity/waveguide modes (0.2–10 mHz) to ion cyclotron fluctuations (0.05–0.5 Hz). Recent studies have analyzed the waves and resonances at ~ 0.8–10 mHz and their propagation toward ionosphere [4–9]. Impacts of interplanetary shocks with the magnetosphere can produce dynamic pressure pulses and waves, propagating upstream from MP to BS [9, 10]. This study is focused on the backward (relative to MP, thus upstream) disturbances propagating towards BS and further into the foreshock. The excitation of the resonances from MP to BS has been identified as triggered by the short wave impulses with the sunward Poynting flux. First time it was detected near MP by INTERBALL-1 and CLUSTER [1, 2, 8]. It was proposed that (with the 3-wave interactions) these impulses can trigger strong jets in MSH flowing around MP, which re-

1) e-mail: ssavin@iki.rssi.ru

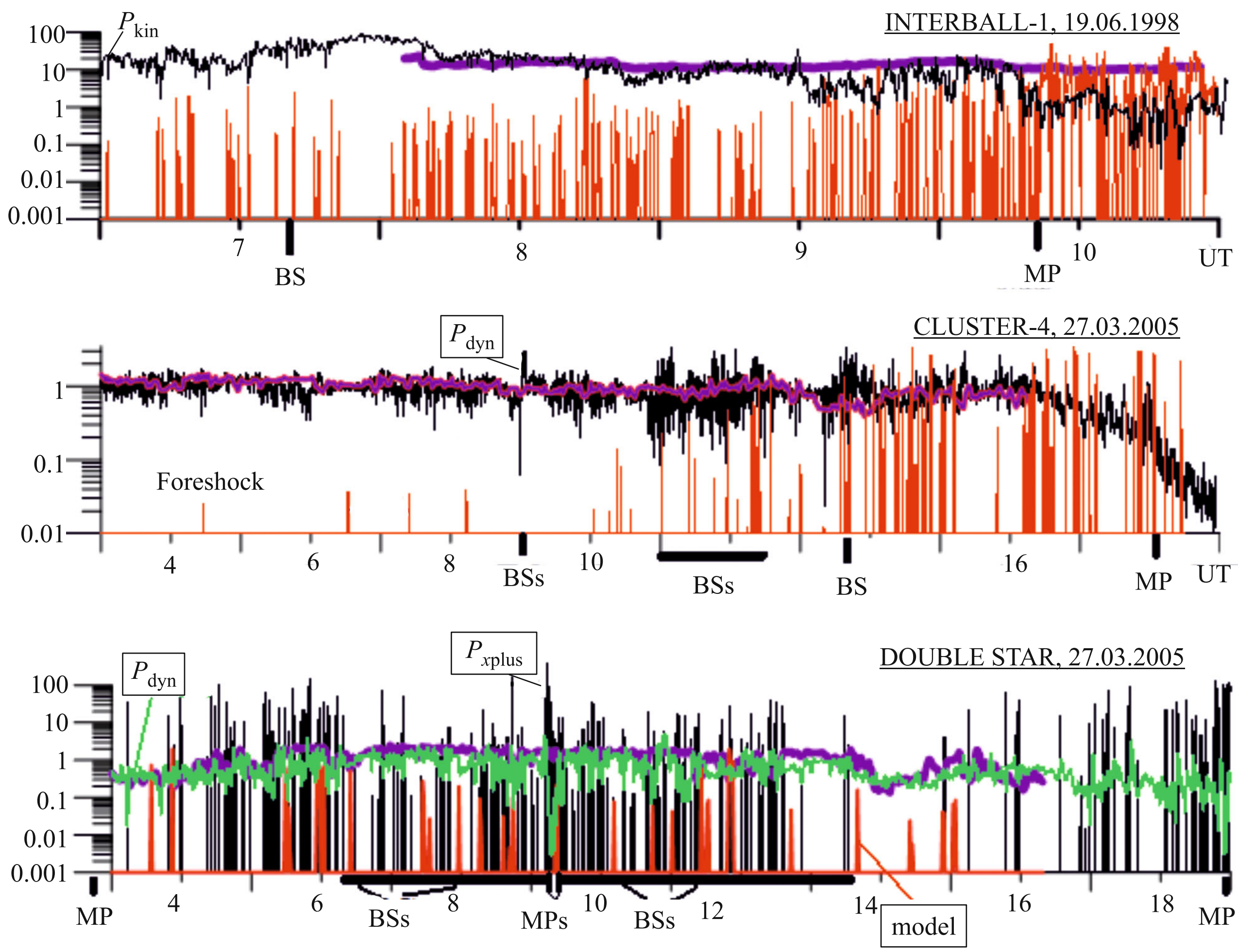

Fig. 1. (Color online) **Top.** Interball-1 (I1), 19.06.1998, thin black line-kinetic energy density $P_{\text{kin}} = P_{\text{dyn}}/2$ (dynamic pressure, [keV/cm^3]), 10 s – sampling; thick violet – Gasdynamic Convected Field model (GDCF) [2, 15], red impulses – sunward Poynting flux $P_{x\text{plus}}$ (relative values from filtered ion velocity and magnetic field data). **Middle.** Cluster-4 (C4) 27.03.2005, similar to I1 excluding 4 s sampling; P_{dyn} in [nPa] and MHD model [5] at 03–16:30 UT with 1 min sampling. **Bottom.** Double Star (DS) 27.03.2005, thin green line-dynamic pressure P_{dyn} (in [nPa] averaged for 1 min); thick violet line MHD model, thin black impulses $P_{x\text{plus}}$ (4 s sampling), thick red impulses $P_{x\text{plus}}$ – from MHD model [5]. BS – bow shocks, MP – magnetopauses

duces the normal to MP flow in its vicinity down to the Alfven speed, thus creating, e.g., conditions for sunward motion of the MP [1–3, 8, 11]. The sunward Poynting flux bursts could trigger surface waves at BS, which in turn modulate the jet production at the BS, deformed by the surface waves [1–3, 14]. The sunward – propagating electric field impulses can also decelerate the MSH plasma in the vicinity of MP in the Sun-Earth direction by the ion finite-gyroradius effects and inertial drift [2]. The question then is if these processes, involving nonlinear waves, control the dynamics and resonances up to BS? In order to answer this question we analyze data on 27.03.2005 from CLUSTER-4 (C4), DOUBLE STAR TC1 (DS; DS was in low-latitude MSH for 17 hours; these data were obtained for the period when the DS spacecraft spent a long time in the MS near a subsolar fairly uniform domain in magnetosheath), INTERBALL-1 (I1), which cover the main interaction regions from the bow shock to the outer cusp, and compare them with gasdynamics and MHD models.

Waveform data and models. The gasdynamic convected field model GDCF (I1, see caption of Fig. 1 and [15]) describes plasma flow for fixed from the experiment MP and BS (detected by a spacecraft) and adds the frozen-in magnetic field from in situ SW data. As shown in Fig. 1, such model reproduces P_{dyn} till MP, with some overestimation in the zone of the jet generation at ~0.9–10 UT [1], with the jets carrying substantial part of the MSH momentum around MP [1, 2]. Figure 1 demonstrates much more impulses of $P_{x\text{plus}}$

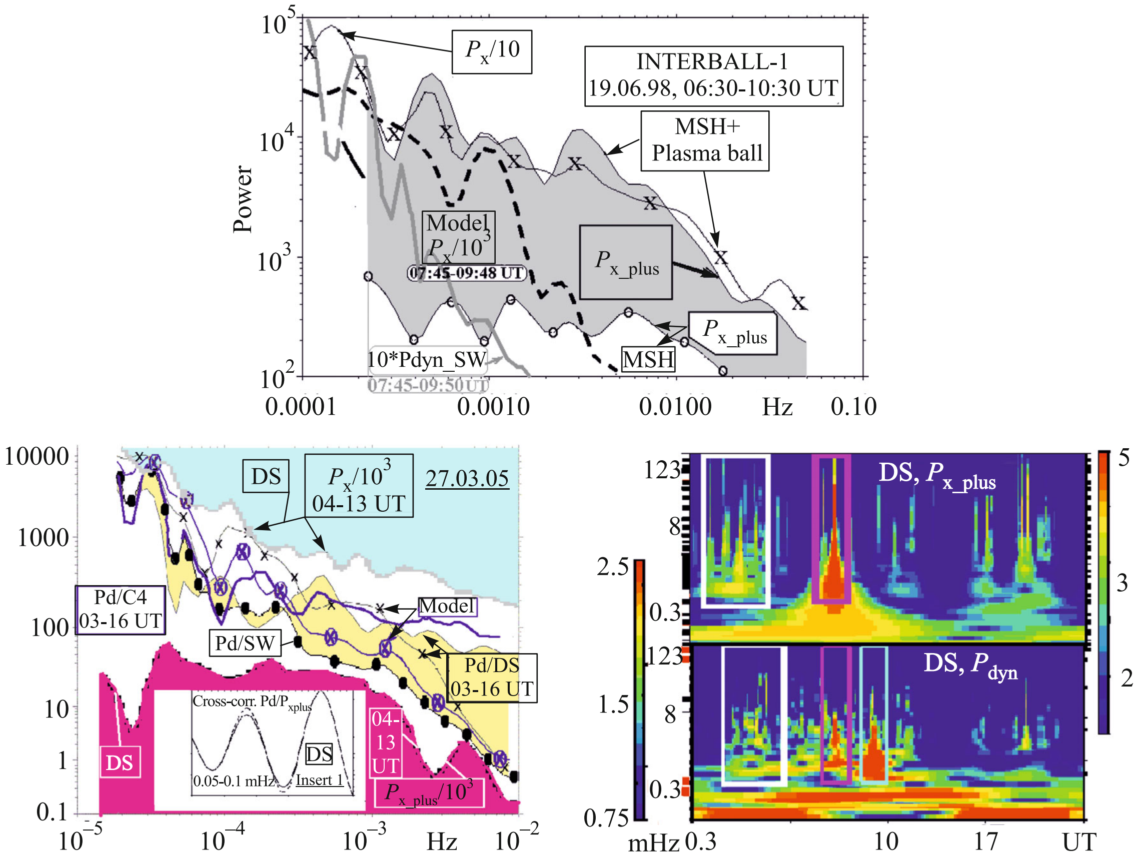

Fig. 2. (Color online) Wavelet power spectra of $P_{\rm dyn}$ (denoted $P_{\rm d}$). Poyting flux in X direction P_x and its component to the Sun, $P_{x\rm plus}$ (see Fig. 1 caption) wavelet power spectra. **Left:** I1, for 06.30–10.30 UT (excluding intervals labeled in the Fig. 1); dashed – GDCF model P_x ([15], see text); (MSH + PB) = 07.10–10.30 UT (see Fig. 1), MSH = 07.10–09.52 UT. **Center:** C4 & DS model and in situ spectra. **Inset:** cross-correlation of $P_{\rm dyn}$ and $P_{x\rm plus}$ at 03–20 UT; dashed line – the same for 03–13 UT; the signals being filtered in 0.05–0.1 mHz range by the 5$^{\rm th}$-order SWAN filter. **Right:** wavelet spectrogram of DS $P_{x\rm plus}$ MSH; (**top**) vertical axis – log-scale frequency 0.03–123 mHz (red digits), color log-power scale – to the right; **bottom:** the same for $P_{\rm dyn}$, the color scale – to the left

compared to the earlier papers [1, 2], which became evident due to the use of the logarithmic scale. GDCF model (projected on the I1 orbit) doesn't reproduce $P_{x\rm plus}$ (only 2 spikes, not shown).

An MHD model that uses the SW data with the resolution of 1 min as the input [5], projecting the model data on the spacecraft orbits, was used for comparison with the DS and C4 data. It shows impulses $P_{x\rm plus}$ (red thick lines, bottom panel, 03–16:20 UT). The data from C4 are displayed with 4 s resolution, while for DS the data are averaged over 1 min. The MHD model [5] reproduces fairly well the data averaged over 1-min. It does not show the most numerous spikes in $P_{\rm dyn}$, the jets [3], while in the averaged DS signal $> 70\,\%$ jets also disappear (versus C4 data in Fig. 1 and original DS data with the same 4 s resolution). Similar to the I1, $P_{x\rm plus}$ impulses (black) are concentrated near BS and upstream of MP. The C4 (middle panel) demonstrates weak $P_{x\rm plus}$ spikes in the foreshock and again in the BS and upstream MP regions. Earlier studies [1–3, 8, 11] infer that the jets can play a major role in the MSH dynamics (see also [14] as an independent review). Here we don't discuss the cause-effect relationship between these jets and waves. Note that the jets in MSH have $P_{\rm dyn}$ are usually larger than that in SW (in $\sim 70\,\%$), so they should determine the energetics of the interactions in MSH [11].

Spectral features. Figure 2 (left panel, I1) shows $P_{\rm dyn}$ in SW (grey line) that seems to provide tracking the MSH maxima (with smoothing) till ~ 0.5 mHz. Grey line in Fig. 2 (left panel, I1) shows $P_{\rm dyn}$ in SW. It behaves somewhat similarly to the MSH line (below grey shading) up to about 0.5 mHz. However, there is also a notable difference, i.e., sharp peaks in $P_{\rm dyn}$ absent in MSH, which implies the influence of local factors in addition to direct SW driving. The model P_x (dashed line) displays local resonances (poorly visible in SW) at 1 and 2.2 mHz. The real P_x (crosses) follows fairly well the model results for 1 mHz. Resonant peaks at 0.5, 1, and 3 mHz are observed in both P_x and $P_{x\mathrm{plus}}$ in MSH and outer cusp (called in [2] "Plasma Ball", PB, grey shadowing). In MSH the resonant frequencies differ (circles), the level is much weaker than in MSH plus PB (gray shadowing). The latter seems to confirm the conclusion that in PB the sunward going waves control the boundary between MSH and PB [1]. It also indicates a role in the interaction with SW on global scales (cf. P_x). It looks strange that $P_{x\mathrm{plus}}$ has different resonances in MSH and PB. The nature of the local GDCF resonance at ~ 1 mHz should be further clarified as we do not find regular impulses in the GDCF model $P_{x\mathrm{plus}}$, so a different physics should be involved (BS/MP eigen modes?).

The P_{dyn} from the MHD model and spacecraft data are shown in Fig. 2 (middle panel, DS, C4), and they track the SW values up to 0.07 mHz. Further, the dominant role of local resonances is seen in the data. The P_x data from DS near BS (cyan upper shading) poorly correlates with both SW and model P_{dyn} (excluding the model maximum at ~ 0.1 mHz) indicating dominance of local resonances. $P_{x\mathrm{plus}}$ correlates weakly with P_x and all P_{dyn}, excluding ~ 0.05 mHz in P_x. The spectrograms on the right panel of Fig. 2 demonstrate similarities among the $P_{\mathrm{dyn}}/P_{x\mathrm{plus}}$ spectra till ~ 15 UT. In the top right panel of Fig. 2, near 0.03–0.1 mHz the horizontal maxima are seen. We filtered the data at 0.05–0.1 mHz with the filter of 5$^{\mathrm{th}}$ order and calculate correlations between P_{dyn} and $P_{x\mathrm{plus}}$ (using SWAN, see inset 1); there are 3 maxima at the time shifts: $\sim +7000$ s with 93 % correlation maximum (corresponds to 0.14 mHz, 03–20 UT, which could be the fundamental BS surface mode), -4300 s/64 % (dashed line, $\Leftrightarrow$ 0.24 mHz, 03–13 UT, BS surface harmonic and/or coupling with the MP surface mode) and $+1744$ s/-80 % ($\Leftrightarrow\sim$ 0.5 mHz, 03–13 UT, which could be MP surface mode and/or a BS harmonic). So, we suggest that at BS surface modes govern the resonant process (note positive signs of the respective time shifts), while at the MP, a, say, surface mode (negative shift) adds a reverse-loop connection between magnetosphere (or MP) and BS. The time lag of the MP surface mode in the band of 0.05–0.1 mHz suggests strong interaction between the MP and BS modes, and initiation of the resonances near MP (cf. Fig. 3). The spikes at the higher frequencies in the right panel of Fig. 2 are seen at 0.4–15 mHz at $\sim$ 04–06 UT (white frames). The spikes have the periodicity corresponding again to ~ 0.5 mHz that is close to the horizontal maximum at 04–06 UT. The continuous horizontal maxima at ~ 0.5 and 0.8 mHz look to "glue" the bursts, with the signal at ~ 0.8 mHz being coherent during more than 3 periods (SWAN). In the P_{dyn} very similar coherent structure at 0.4–15 mHz (white frame) is delayed by the time lag corresponding again to the resonance at $\sim$0.5 mHz. We suggest that this coherent structure launches the BS disturbances, followed by the global coherent resonances throughout BS/magnetosphere. After the nearly simultaneous spectral spikes at ~ 09 UT (violet frame), the larger jet activity starts. An intensive spectral spike in P_{dyn} (blue frame) has no counterpart in $P_{x\mathrm{plus}}$ corresponding to the BS becoming a quasi-perpendicular shock [3]. In this case the BS undergoes a reformation with a "trigger" directly from SW. DS wavelet cross-spectrograms of $P_{x\mathrm{plus}}$ and P_{dyn} (not shown) demonstrate nearly constant correlation at 0.02–0.06 mHz. This supports that the $P_{x\mathrm{plus}}$ can trigger the BS processes, which in turn can modulate the jets hitting the MP.

3-wave nonlinear interactions. Earlier analysis of the data of I1 on 19.06.1998 [1, 2] yielded the first demonstration of possible 3-wave interaction near MP triggered by the sunward-propagated waves, and now we present the clear confirmation of this effect by bi-spectra in Fig. 3. It was found that for the bi-coherence the horizontal maximum (inferring a nonlinear cascade [1–3]) at $\sim$ 5–6 mHz strongly dominates near MP (middle top panel in Fig. 3, the same for 09–09:47 UT, not shown). A weaker maximum exists in the outer MSH till BS (left top panel) at slightly smaller frequency. There the dominant horizontal bi-maxima are detected at ~ 0.3, 0.5 and 1 mHz, along with the weaker ones at ~ 2 and 3 mHz (it differs from near-MP, middle panel, cf. Fig. 2). Note that the unusually high bi-coherence value > 70 % is due to our physical choice of bi-coherence analysis inputs (see Fig. 3 caption), especially of the strongly nonlinear impulsive signal of $P_{x\mathrm{plus}}$. Figure 3 right top panel demonstrates the extended reservoir of the heated MSH plasma – the PB (the stagnant outer cusp with heated MSH plasma [2]). The 3-wave interaction picture completely differs from the top middle panel (excluding ~ 1 mHz). It agrees with the conclusion from the results in Figs. 1 and 2, that the local nonlinear interactions control the boundary at the cusp outer edge [2]. At the same time for ~ 3 and 0.1 mHz, the left and right top panels display more similarities, inferring the global influence of PB on the SW plasma streaming around the magnetosphere. C4 bi-spectra near MP (middle right panel) are almost the same as in the I1 case (middle top), confirming the specific nonlinear-interaction zone in front of MP. Its outer boundary [13] relay with "slow shock". In the near-BS MSH (middle, cf. top left) the bi-spectra again resemble I1 case, with

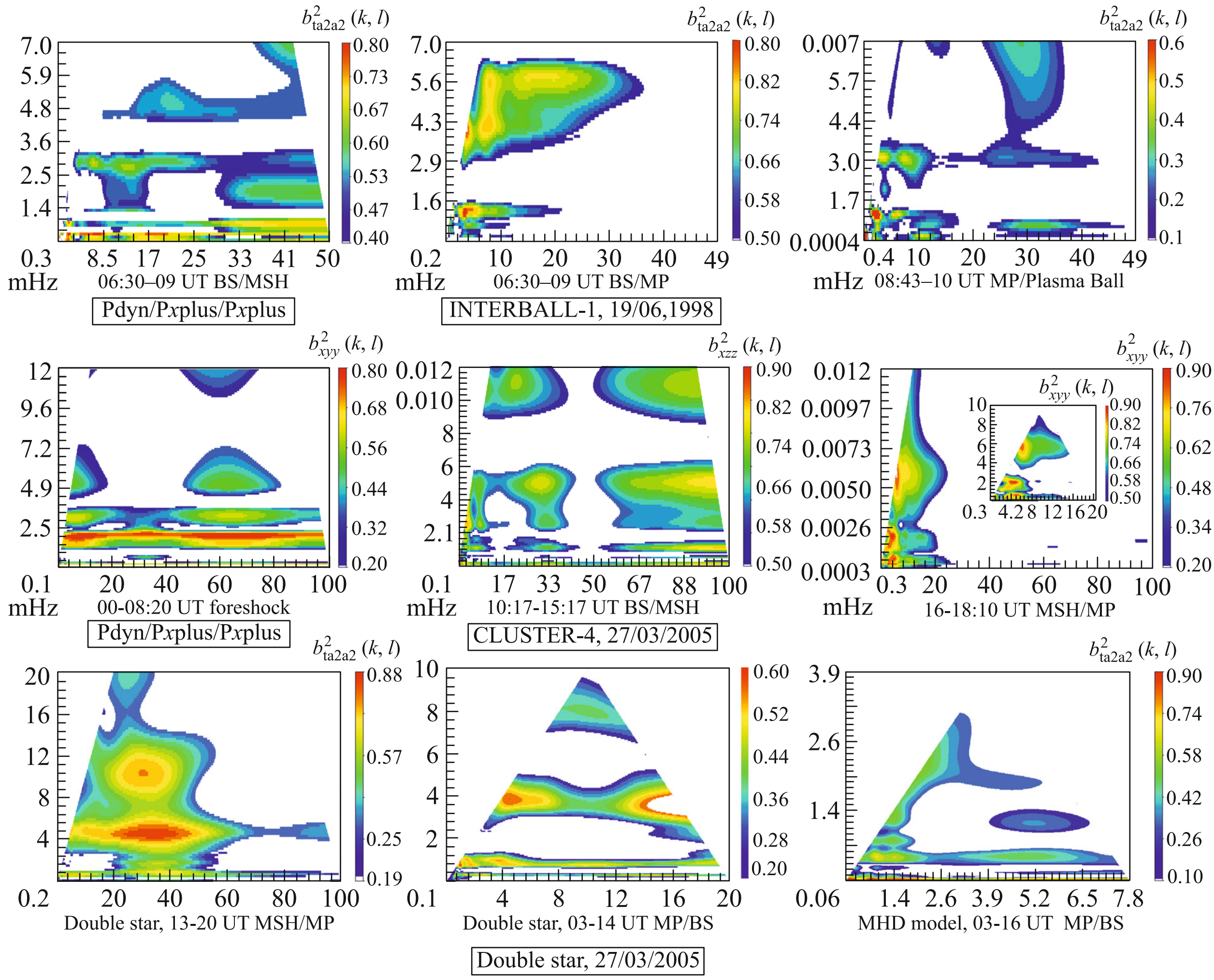

Fig. 3. (Color online) Wavelet bi-spectra ($F_{\rm vertical} + F_{\rm horizontal} = F_{\rm sum}$ (not shown); inputs: $P_{\rm dyn}/P_{x\rm plus}/P_{x\rm plus}$, see text). From top/left to right: I1 BS/MSH; I1 BS/MP; I1 MP-Plasma Ball (PB) [2]; **Middle:** C4 foreshock; C4 BS/MSH; – C4 MSH/MP (+blow up); **Bottom:** DS MSH/MP; DS MP/BS; MHD model

a new maximum at ~ 11 mHz (at higher sampling). C4 did not cross PB but surprisingly displays quite strong 3-wave interactions in the foreshock (middle left). The real C4 data in the foreshock displays quite strong 3-wave interactions. The real C4 power spectra in the foreshock display local resonances at > 0.5 mHz which reasonably correspond to the simultaneous ones in MSH on DS (not shown), indicating substantial influence of the foreshock on the SW interaction with MP. While the model $P_{\rm dyn}$ on C4 in Fig. 1 follows the real one, the model DS $P_{\rm dyn}$ overestimates a bit the real one, inferring that SW pre-dissipation in the foreshock might be non-MHD one [2, 8]. One couldn't anticipate so clear and large (up to 90 %) bi-spectral maxima in the foreshock at the discrete frequencies for the $P_{x\rm plus}$ (trigger) and in wideband for the $P_{\rm dyn}$ (i.e., cascade-like [1–3, 8, 11]), which carries the dominant energy in the foreshock and MSH. After BS involved into the eigen magnetospheric oscillations by $P_{x\rm plus}$ impulses, the oscillations are manifested from BS to the near geotail, and seem to be driven in MSH by the respectively modulated plasma jets [3]. Inertial drift and nonlinear Cherenkov resonance in the foreshock are alternatives to the deformed BS in the plasma jets' production in the magnetosheath [1–3, 14]. Near MP the bi-spectra on DS (bottom left) are compatible with the C4 and I1 cases, with small difference in frequency values at low values. At ~ 10 mHz an extra maximum is seen. In the MSH and BS sliding region by DS (Fig. 3, middle bottom) a low-frequency (~ 8 mHz) horizontal line exists. Peaks at 3–5 and 0.7–1 mHz resemble the near-MP cases. The MHD model [4] (bottom right) is limited on vertical axis by ~ 4 mHz (sampling 1/min). The horizontal maxima at ~ 0.5 and 0.07 mHz are reasonably close to the observed cases (~ 0.7–1 and 0.05 mHz, bottom middle).

Results. The digital-like impulses in $P_{x\text{plus}}$ (their nature to be explored in details in the future, cf. [13]) provoke the strongest ($>80\,\%$) 3-wave cascade-like interactions (cf. horizontal maxima in Fig. 3); it can result in appearance of jets [3, 14]. The MHD model confirms the decisive role of the upstream propagating waves in MSH and strong 3-wave interaction as the discovered mechanism of deceleration and deflection of the SW flow at the bow shock and in MSH. The foreshock bi-spectra infer that the nonlinear Cherenkov resonances (induced scattering?) and/or inertial drift, which we introduced as a source for the near-MP jets and interactions [11], could operate also in the foreshock. So, the jets can be produced not only by a deformed bow shock [14].

We demonstrate the following new results:

1. Strongly nonlinear waves (impulses in the sunward Poynting flux) are acting to reduce the dominant dynamic pressure of the solar wind at the geomagnetic boundaries via the strong nonlinear 3-wave interaction.

2. There are 4 zones of the nonlinear interactions:

– bow shock;

– pre-magnetopause deflection region [2, 3];

– "Plasma Balls" – the outer cusp throat [3] with the negligible role of the DC magnetic field at the outer border of cusp. Instead, a turbulent barrier separates the flowing and stagnant plasmas [2];

– foreshock which starts to trigger the interactions.

3. The resonances from magnetopause can be transported back to bow shock namely by the demonstrated spikes observed in $P_{x\text{plus}}$.

4. The MHD model [4] qualitatively reproduces the nonlinear physics of the solar wind interaction with geomagnetic field in the region from the bow shock to the magnetopause.

Earlier studies [1–3, 8, 11] have shown that the modulation by the resonant jets can be a general effect in the magnetospheric physics. But the poor agreement with the MHD model highlights the need to clarify further the role of the jets in the solar wind interaction with magnetosphere.

We thank Valery Smirmov for providing SKA-1 ion data used in the calculations of the dynamics pressure on I1 and Paul Song for GDCF model. The spacecraft and OMNI data were downloaded from the CDAW Website. The spectral and correlation analysis used the SWAN software, made available by LPCEE staff. We regret that Ermanno Amata participated only in the beginning of the paper writing, he also provided DS and C4 ion data. We thank Prof. Mark Koepke and his team for validating of our bi-spectral analysis. ISSI supported one meeting of Savin/Wang Team on the paper topic.

1. S. P. Savin, L. M. Zelenyi, E. Amata, J. Buechner, J. Blecki, S. I. Klimov, B. Nikutowski, J. L. Rauch, S. A. Romanov, A. A. Skalsky, V. N. Smirnov, P. Song, and K. Stasiewicz, JETP Lett. **79**, 452 (2004).
2. S. Savin, A. Skalsky, L. Zelenyi et al. (Collaboration), Surv. Geophys. **26**, 95 (2005).
3. S. Savin, E. Amata, V. Budaev, L. Zelenyi, E. A. Kronberg, J. Buechner, J. Safrankova, Z. Nemecek, J. Blecki, L. Kozak, S. Klimov, A. Skalsky, and L. Lezhen, JETP Lett. **99**, 16 (2014).
4. A. S. Leonovich, V. A. Mazur, and D. A. Kozlov, in *Low Frequency Waves in Space Plasmas, Geophysical Monograph* **216**, 151, American Geophysical Union and John Wiley and Sons, Inc (2016).
5. Y. Q. Hu, X. C. Guo, and C. Wang, J. Geophys. Res. **112**, A07215 (2007); doi:10.1029/2006JA012145.
6. V. M. Nakariakov, V. Pilipenko, and B. Heilig, Space Sci Rev. **200**, 75 (2016); doi:10.1007/s11214-015-0233-0.
7. F. Plaschke, H. Hietala, V. Angelopoulos, and R. Nakamura, J. Geophys. Res. **121**, 3240 (2016); doi: 10.1002/2016JA022534.
8. S. Savin, E. Amata, M. Andre et al. (Collaboration), Nonlin. Processes Geophys. **13**, 377 (2006); doi:10.5194/npg-13-377-2006.
9. G. Pallocchia, J. Geophys. Res. **118**, 1125 (2013); doi:10.1029/2012JA017851.
10. G. Pallocchia, A. A. Samsonov, and M. B. Bavassano, Ann. Geophys. **28**, 1141 (2010); doi:10.5194/angeo-28-1141-2010.
11. S. Savin, L. Zelenyi, E. Amata et al. (Collaboration), Planet Space Sci. **53**, 133 (2005).
12. P. Song, C. T. Russell, and M. F. Thomsen, J. Geophys. Res. **97**, 8295 (1992).
13. K. Stasiewicz and C. Z. Cheng, Ann. Geophys. **7**, 4379 (2009).
14. F. Plaschke, H. Hietala, M. Archer, X. Blanco-Cano, P. Kajdiyc, T. Karlsson, S. Hee Lee, N. Omidi, M. Palmroth, V. Roytershteyn, D. Schmid, V. Sergeev, and D. Sibeck, Space Sci. Rev. **214**, 81 (2018).
15. P. Song, C. T. Russell, T. I. Gombosi, J. R. Spreiter, S. S. Stahara, and X. X. Zhang, J. Geophys. Res. **104**, 345 (1999).